ENSA/DOE Test Plan Modeling and Analysis Support

Spent Fuel and Waste Disposition

Prepared for
US Department of Energy
Spent Fuel and Waste Science and Technology
Nicholas A. Klymyshyn,
Pavlo Ivanusa, Kevin Kadooka,
David Garcia, Justin Smith
Pacific Northwest National Laboratory

September 30, 2017
SFWD-SFWST-2017-000035
National Laboratory Report No. PNNL-26912

Reviewed by:

Project Manager – Brady Hanson

Brady Hanson (Signature on File)
Name

This page is intentionally left blank.

SUMMARY

This report summarizes the modeling and analysis work done by Pacific Northwest National Laboratory (PNNL) to support the Equipos Nucleares Societdad Anónima/U.S. Department of Energy (ENSA/DOE) test campaign during fiscal year (FY) 2017. The purpose of the ENSA/DOE test campaign is to study the shock and vibration loading conditions that spent nuclear fuel can be expected to experience during normal conditions of transport over many different modes of transportation, as well as the handling loads that occur when changing from one transportation mode to another. Modeling and analysis are key components of the overall test campaign, contributing to the design of the test configuration and instrumentation plan, forming pre-test predictions, evaluating the data once it is collected, and ultimately projecting the as-tested response data into predictions of real, irradiated spent nuclear fuel rod behavior. This report describes five different modeling and analysis activities that were completed this FY. These modeling and analysis activities are valuable to different phases of the test campaign. Pre-test predictions of a planned railcar test were made to establish expectations going into the test. Finite element modeling of simulated fuel assemblies was done to estimate their vibration frequency range response and to prepare for future modeling of the full fuel basket. Data processing scripts and algorithms were developed to start processing data as it was collected this FY. Fatigue damage evaluation tools were developed to calculate potential cladding fatigue damage from strain gage data. Finally, an evaluation of accelerometer data was performed to assess the behavior of the rubber pads used between the cask and cradle structure and the flat railcar deck. This report fulfills the M3 milestone M3SF-17PN010202032 “Finite Element Modeling Support” under work package SF-17PN01020203.

A pre-test prediction of the pitch and bounce railcar test performed at Transportation Technology Center, Inc. (TTCI) was made using numerical models. A peak strain of about 300 microstrains (μE) was predicted. This will be compared in detail with the actual test data when they become available, so that the models can be improved as necessary to achieve the best agreement with test data.

Simulated fuel assemblies were used in 29 of the 32 fuel locations of the ENUN 32P dual purpose cask during the ENSA/DOE test campaign. The simulated fuel assembly design was modeled and analyzed. It was determined that the dynamic response of the simulated fuel assemblies is expected to have characteristic frequencies near 5 Hz and 55 Hz. These two frequencies could appear in the test data, particularly in the basket accelerometers.

PNNL developed software tools to process the many terabytes of data that will come from the ENSA/DOE test campaign. The tools are demonstrated on a preliminary data set.

PNNL also developed cladding fatigue evaluation tools for calculating fatigue damage from strain gage data. The process was illustrated using a 34-hour data set that is representative of normal conditions of transport shock and vibration. The analysis predicts cladding fatigue damage for normal conditions of transport that is approximately zero.

Extra accelerometers were added for some of the TTCI tests to study the effect of the rubber pads that were placed between the railcar deck and the cask’s cradle. The data were evaluated and the pad was determined to have a frequency-dependent effect on load transmission. The difference in acceleration magnitude between the railcar deck and the cask cradle is a factor between 0.3 and 2 that varies over the frequency range of interest. From 0 Hz to 20 Hz there is an amplification of loads, from 20 Hz to 60 Hz there is an attenuation of loads, and above 60 Hz there is no effect.

This page is intentionally left blank.

CONTENTS

This page is intentionally left blank.

LIST OF FIGURES

This page is intentionally left blank.

ACRONYMS

CAD	computer-aided design
DOE	U.S. Department of Energy
ENSA	Equipos Nucleares Sociedad Anónima
FY	fiscal year
PNNL	Pacific Northwest National Laboratory
RMS	root mean square
TTCI	Transportation Technology Center, Inc.
µE	microstrain, .000001 mm/mm

This page is intentionally left blank.

1. INTRODUCTION

This report summarizes the modeling and analysis work done by Pacific Northwest National Laboratory (PNNL) to support the Equipos Nucleares Societdad Anónima/U.S. Department of Energy (ENSA/DOE) test campaign during fiscal year (FY) 2017. The purpose of the ENSA/DOE test campaign is to study the shock and vibration loading conditions that spent nuclear fuel can be expected to experience during normal conditions of transportation over many different modes of transportation, as well as the handling loads that occur when changing from one transportation mode to another. Modeling and analysis are key components of the overall test campaign, contributing to the design of the test configuration and instrumentation plan, forming pre-test predictions, evaluating the data once it is collected, and ultimately projecting the as-tested response data into predictions of real, irradiated spent nuclear fuel rod behavior. This report describes five different modeling and analysis activities that were completed this FY. These modeling and analysis activities are valuable to different phases of the test campaign. Pre-test predictions of a planned railcar test were made to establish expectations going into the test. Finite element modeling of simulated fuel assemblies was done to estimate their vibration frequency range response and to prepare for future modeling of the full fuel basket. Data processing scripts and algorithms were developed to start processing data as it was collected this FY. Fatigue damage evaluation tools were developed to calculate potential cladding fatigue damage from strain gage data. Finally, an evaluation of accelerometer data was performed to assess the behavior of the rubber pads used between the cask and cradle structure and the flat railcar deck. The five different modeling and analysis activities are described in more detail in the following paragraphs, and they are followed by a discussion of the magnitude of strains expected in this work.

Section 2.0 describes pre-test predictions for one of the captive track tests performed at the Transportation Technology Center, Inc. (TTCI). This analytical effort combines a railcar dynamics simulation with the linear structural models of the cask and conveyance, and nonlinear models of the fuel assembly. The set of models is a starting point. Validation against the test data should provide insight into how the numerical models can be improved in the future.

Section 3.0 describes finite element modeling of the simulated fuel assemblies that were used during testing. The ENSA ENUN 32P dual-purpose cask normally carries 32 fuel assemblies in a basket structure. During the ENSA/DOE test campaign, three of the 32 fuel assembly locations contained surrogate, instrumented fuel assemblies with fuel rods that contained surrogate mass instead of real, irradiated fuel pellets. The remaining 29 basket locations were filled with simulated fuel assemblies that were specially designed and constructed for this test campaign. The simulated fuel assemblies were designed to have the same mass as a real fuel assembly, but are otherwise very different from a structural standpoint. Models of the simulated fuel assemblies are needed for fuel basket level modeling of the cask. Analyses of the simulated fuel assemblies explored their dynamic response characteristics.

Section 4.0 illustrates the data processing steps being developed at PNNL to process the many terabytes of data that were generated during the ENSA/DOE test campaign. Automation is key to studying such a large data set and extracting useful information. The process is still under development, but this section provides insight into its use and results.

Section 5.0 discusses PNNL's fatigue damage calculation tools, and applies them to a representative set of strain gage data. Final test data are not yet available, but the representative data set provides a prediction of the magnitude of cladding fatigue damage that is expected of the real data.

Section 6.0 evaluates extra accelerometer data that were collected at TTCI to study the effect of the rubber pad that was used between the railcar deck and the cask cradle. The pad was added by the shipping company as a standard operating procedure. It was suspected that it could have a damping or attenuation effect on the loads transmitted from the railcar to the cradle and cask.

The strains discussed in this report are so low relative to normal engineering strains that it is most convenient to report them in microstrains (μE). One μE equals 0.000001 mm/mm of strain. In normal engineering applications, strains are typically reported as unitless numbers or percentages. A strain of 1% is equal to 10,000 μE. Irradiated zirconium alloy cladding has a failure strain that is on the order of 10,000 μE. The peak cladding strain recorded during normal conditions of transport testing has tended to be on the order of 100 μE, or two orders of magnitude below the failure limit. Finite element modeling predictions tend to be conservatively higher than recorded test data—in the broad range of 300 μE to 750 μE—or within an order of magnitude error. A major goal of this work is to validate the numerical models against test data to provide confidence that the models can predict the behavior of different fuels carried in different conveyance systems.

2. PRE-TEST PREDICTIONS

A pre-test prediction was made using NUCARS, ANSYS, and LS-DYNA software to simulate the response of surrogate fuel rods when the assemblies are subjected to normal conditions of transport within the ENSA Transport (ENUN) 32P cask. The modeling method is illustrated in Figure 1. NUCARS simulated the railcar crossing the pitch and bounce test track at TTCI. ANSYS was used to calculate the load transmission through the cradle to the cask. LS-DYNA was used to calculate the response of the fuel cladding to pitch and bounce loads. The analysis was documented in two conference papers (Klymyshyn 2017 and Jensen 2017) as summarized here.

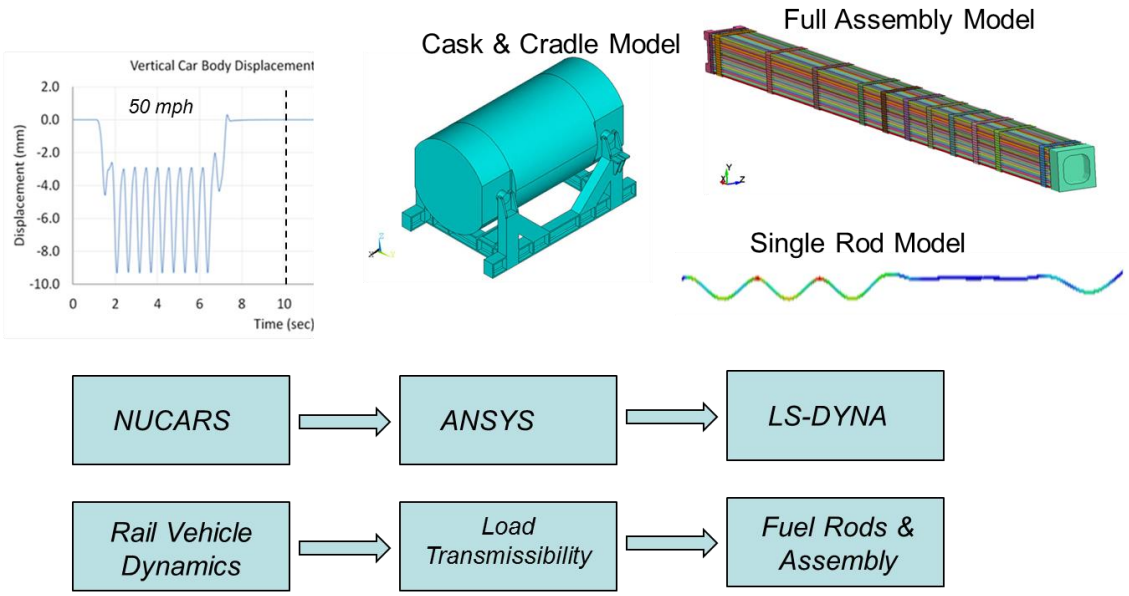

Figure 1. Pretest Prediction Modeling Method

The NUCARS model assumed the conveyance was a Kasgro 370-series 12-axle railcar. Twelve axles were selected to match the Atlas railcar, which is currently under development. The specific railcar model had not yet been identified when the pre-test analysis was completed, but it turned out that the Kasgro 370 series was a good guess. The actual railcar was a Kasgro 370355, so the pre-test predictions used a good approximation.

An interesting observation from the NUCARS model results was that the springs of the Kasgro 370-series railcar were relatively stiff compared to the load of the cask and cradle. The "370" indicates a carrying capacity of 370 tons (740,000 pounds or 336,000 kg), but the cask and cradle only weigh about half of that capacity. As a consequence, the railcar springs only deflected a small fraction of their total capacity. A purpose-built railcar designed to carry the cask and cradle would be expected to have larger spring deflections, so a second case, with half the spring constants, was analyzed. The full spring case was analyzed as a pre-test prediction, while the half-spring case was run to see how sensitive the cladding strains were to the spring constant. The results of the half-spring case suggest that the cladding strains are not very sensitive to the railcar spring constant; peak strain increased by about 15% from a 50% change in spring constant.

The NUCARS results predicted the dynamic response history of the pitch and bounce at a speed of 50 mph. The simulation used the track profile of the TTCI pitch and bounce track. The dynamic response calculated at the railcar center-bowls (the two locations where the flat railcar deck is supported by 6 axels at each end) was used to load an ANSYS structural-dynamic model of the cask and cradle. The ANSYS model used linear mode superposition methods and calculated the dynamic load transmission through the

cask and cradle. The model results predicted a nearly rigid body response, indicating that no significant elastic deflections of the cradle were expected under the pitch and bounce conditions. There was also a nearly direct load transmission from the bottom of the cradle to the top of the cask; little attenuation, amplification, or phase delay occurred.

The calculated dynamic response of the cask was used as the loading condition in two different LS-DYNA models of the fuel cladding. One model calculated the response of a single fuel rod to loads representing the cask motion. The second model calculated the response of a full fuel assembly to the imposed cask motion. Both models calculated the response over 10 seconds of motion and arrived at comparable cladding strain results.

The single cladding model predicted a peak cladding strain of 300 µE, while the full fuel assembly model predicted a peak cladding strain of 336 µE. The single rod model calculated its results in 5 minutes, while the full fuel assembly model took 10 days of continuous calculation. We concluded that the single rod model provides a good estimate of cladding strain, while the full fuel assembly model calculates the detailed behavior for every individual fuel rod in the assembly. As an example of the detail provided by the full fuel assembly model, Figure 2 shows a map of the peak cladding strain (in µE) at each fuel rod location. The reported peak strain is the maximum value that occurs within the 10-second response at any point along the fuel rod length. The highlighted cells indicate strains in excess of 250 µE to highlight the fact that most of the peak cladding strains are much lower; the average value is 109 µE. Note that the blacked-out cells represent the control rod guide tubes.

102	104	95	101	95	80	87	98	112	91	107	95	85	83	89	102	88
89	92	88	89	99	95	115	101	108	102	91	115	102	79	86	93	92
91	100	111	119	93		116	92		106	106		97	102	106	85	92
98	85	83		106	221	147	100	206	126	93	196	131		99	83	87
89	92	86	106	113	99	79	83	112	102	91	118	119	115	89	102	86
90	90		98	91		83	87		102	89		109	88		115	82
85	85	276	126	118	195	110	88	264	116	89	212	131	85	268	116	87
89	92	107	82	83	100	87	84	86	95	86	101	91	92	93	84	77
81	96		98	85		97	88		109	86		98	85		93	88
85	90	336	156	88	238	124	101	193	130	92	238	131	99	225	122	95
93	95	99	129	87	102	86	93	103	86	91	125	86	88	104	100	89
89	96		93	97		113	84		91	83		99	102		96	92
86	122	150	89	111	318	140	86	172	117	105	226	109	92	97	109	97
89	82	97		89	107	98	91	112	94	94	109	108		103	87	86
111	91	110	174	100		95	108		107	95		104	208	111	93	131
89	116	71	113	109	179	123	104	194	112	119	214	132	89	88	92	112
113	96	102	114	83	80	113	100	94	99	96	83	85	98	87	89	89

Figure 2. Peak Cladding Microstrain Map, Pitch and Bounce 50 mph Pretest Prediction

The 50 mph pitch and bounce test was completed at TTCI in August 2017, but the data are not yet available to compare with the pre-test prediction. Although the pre-test prediction is not expected to precisely match the recorded data, it is expected to be relatively close based on previous modeling experience. A number of modeling assumptions were made to simplify the analysis, including the choice to neglect the dynamic behavior of the fuel basket. The test data should help identify which simplifying assumptions need to be revised to achieve greater physical agreement between the numerical models and test data.

3. SIMULATED FUEL ASSEMBLY FINITE ELEMENT ANALYSIS MODEL

During the test campaign, 3 of the 32 basket locations were filled with surrogate, instrumented fuel assemblies, and the remaining 29 fuel assembly compartments were filled with simulated fuel assemblies. These simulated fuel assemblies were designed and constructed by ENSA this year. ENSA provided the drawings and PNNL began building models and analyzing the dynamic behavior of the simulated fuel assemblies. Finite element models of the simulated assemblies are needed for fuel basket level models.

The simulated assemblies consist of a steel square channel that is filled with rebar-reinforced concrete. The simulated assemblies also have a number of nylon pads that were included to protect the basket at the points of contact. There are many ways to approach the modeling of these features, and a range of options were evaluated.

The simulated fuel assembly's geometry was created using Solidworks to make a three-dimensional (3D) computer-aided design (CAD) model (Figure 3). The 3D CAD model was imported into LS-Prepost as the basis for a finite element model. Different finite element mesh densities were evaluated. Figure 4 shows two different mesh options that were evaluated. A number of other models were considered, including hexahedral element models, shell models, and a number of beam models that represent the structure as a classic beam with a homogenous cross section.

Figure 3. Solidworks Model without Chamfers

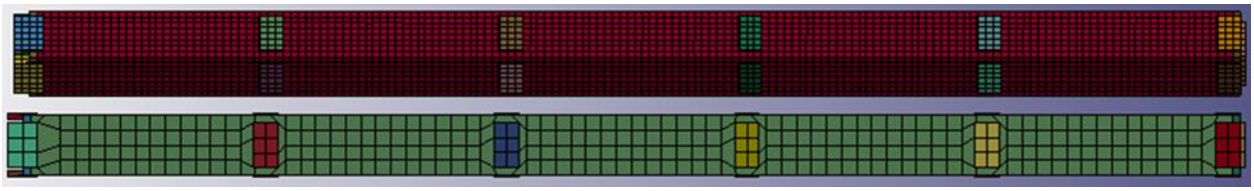

Figure 4. Hexahedral Element Models with Two Characteristic Element Sizes, 0.5 m (bottom) and 0.25 m (top)

One of the most detailed models investigated was comprised of hexahedral elements and accounted for the rebar that exists within the concrete center of the simulated assembly. That model was subjected to sinusoidal acceleration through a rigid surface, which is similar to a fuel assembly responding to the motion of the fuel basket surface it is resting on. Figure 5 shows the maximum displacement response from the simulated fuel assembly model to different amplitudes of excitation. The plot shows that the maximum response occurs around 5 Hz, and a secondary response happens at 55 Hz.

Modal analysis was conducted of the different iterations of the finite element model. The first bending mode occurred in the range of 50–56 Hz, with an average of 53 Hz. This points to the 55 Hz response of Figure 5 as a first bending mode response of the simulated fuel assembly structure. The 5 Hz response of Figure 5 does not align with any significant mode shape, so it is attributed to the nylon pads and the specific boundary conditions of the loading scenario.

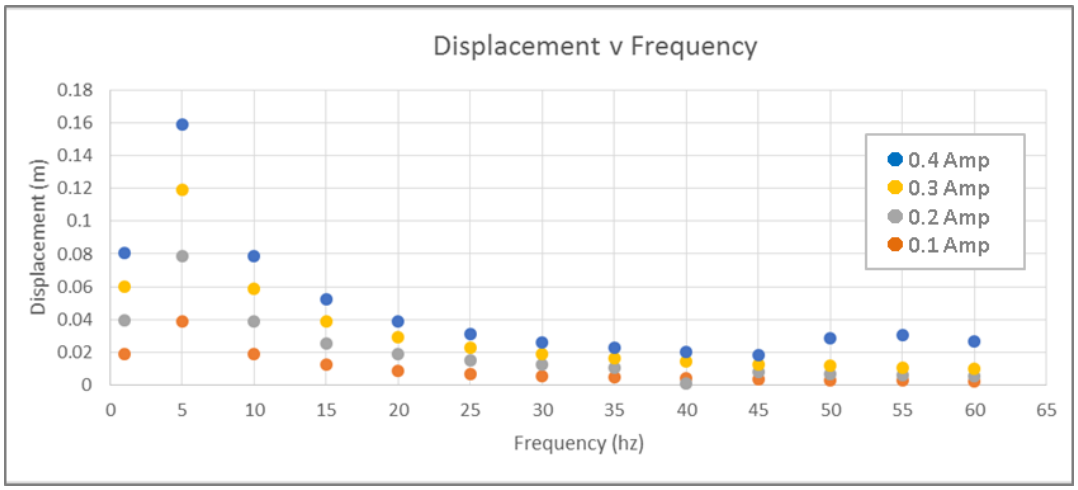

Figure 5. Simulated Fuel Assembly Response to Sinusoidal Excitation

Based on the preliminary modeling, the simulated fuel assembly is expected to have a characteristic response near 5 Hz and 55 Hz. The 5 Hz response is believed to be the mass of the simulated assembly interacting with the nylon pads, similar to a point mass on a spring. The 55 Hz characteristic frequency is a first bending mode response of the long, relatively slender simulated fuel assembly. Of the two, the 5 Hz response is expected to be relatively stronger, but the 55 Hz response aligns with the expected first mode frequency of the cask and cradle system. If significant natural vibration of the conveyance system occurs during testing, the simulated fuel assemblies might also be vibrating at the same frequency. This is something to look for as the data are processed next year. These frequencies could appear in the fuel basket accelerometers, close to their physical location, or elsewhere in the data, such as in the nearby fuel assembly vertical accelerometer data.

4. DATA PROCESSING

PNNL developed strategies for processing the significant amount of data that were collected during the test campaign. PNNL staff started the effort using simulated test data and test data from Sandia National Laboratories' 2014 highway truck test (McConnell et al. 2014). As data from the ENSA/DOE test campaign were received, they were used to develop automated processing scripts and algorithms. By the end of FY 2017, PNNL had developed a preliminary set of tools to filter noise from the data and search for events of interest. Further development and quality assurance are still necessary, and are scheduled to be completed in FY 2018.

All channels of strain gage and accelerometer data have drift in their signal, which can be considered a type of noise that has a long duration. PNNL's preliminary processing strategy is to use a band-pass Butterworth filter to trim the low-end frequency content from the data signals to eliminate drift and to trim the high-end frequency content to eliminate any high-frequency noise in the data.

Figure 6 shows an example of strain gage data from the ENSA/DOE test campaign. Because this is the signal from a strain gage in the cask, the fact that the data signal climbs from zero to a steady 6 µE over the course of 1 hour does not represent any real physical phenomenon. The real shock and vibration component is the short-duration signal that oscillates in a wide band around a "zero value" that climbs from zero to 6 µE.

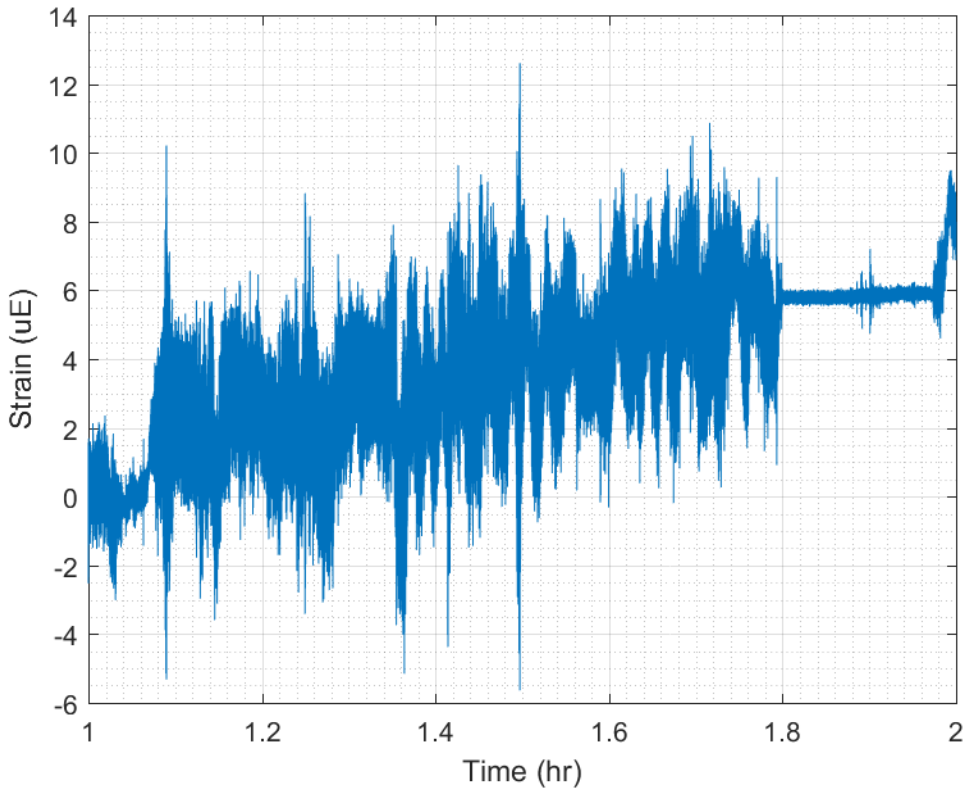

Figure 6. An Example of Raw Strain Gage Data from the ENSA/DOE Test Campaign

Figure 7 shows the raw, unfiltered strain gage signal (Original) in the frequency domain along with the filtered signal (IIR Butterworth). The low-end filter threshold is about 0.1 Hz and the high-end filter threshold is about 100 Hz. The figure illustrates that the low end and high end of the raw data signal are reduced by orders of magnitude, but that the frequency band of interest is not significantly altered. Figure 7 demonstrates that the filter is doing what it is intended to do.

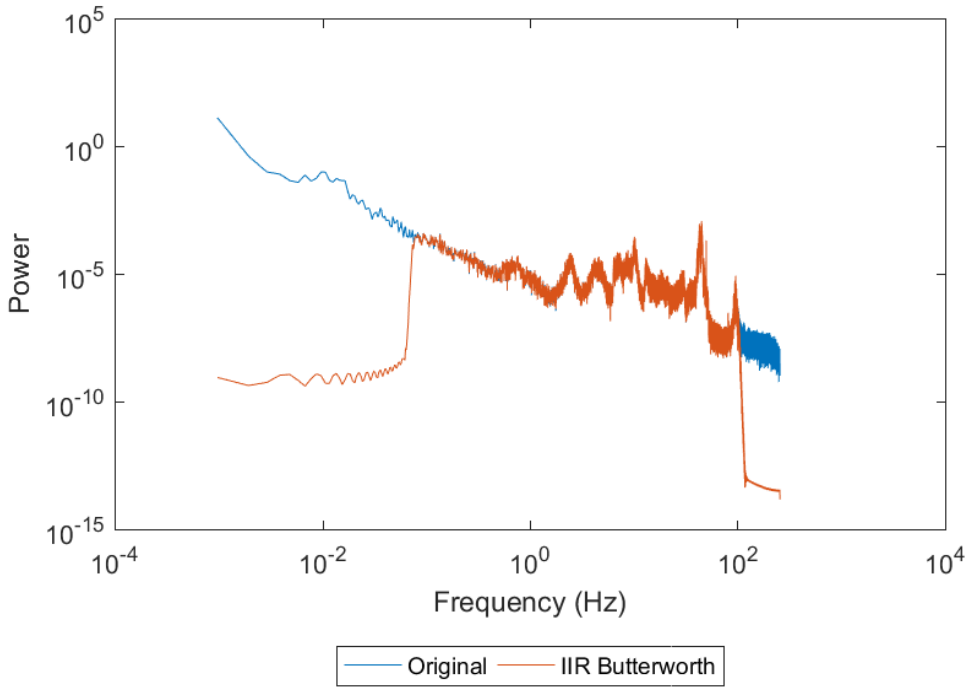

Figure 7. Frequency of Filtered and Unfiltered Stain Gage Data

Figure 8 shows the raw data (Original) plotted with the filtered data (IIR Butterworth). The filter shifts the dynamic strain gage signal to center it on zero. The peak value of the raw data is about 13 µE, while the peak value of the filtered data is about 9 µE. While the change is large from a percentage standpoint, the absolute difference is only 4 µE. The filtered data provide a more sensible view of the cladding response that makes physical sense.

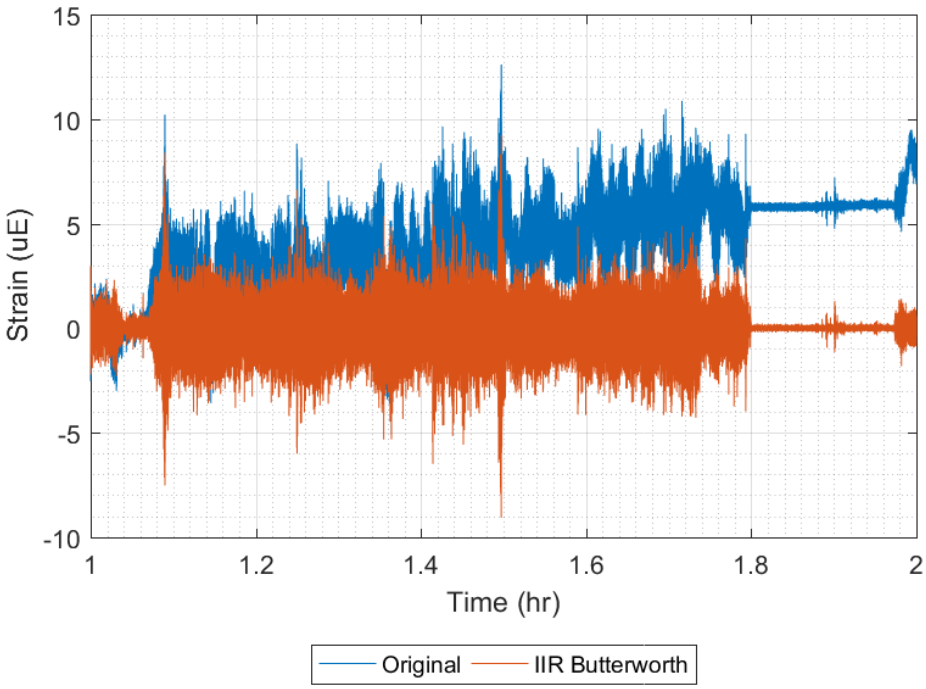

Figure 8. Filtered and Unfiltered Strain Gage Data

While it is easy to find and note the peak instantaneous value in Figure 8, it is also important to determine whether a peak has a significant duration and occurs during a significant transient event, like a mechanical shock event. PNNL's preliminary data processing algorithm uses a root mean square (RMS) operation to determine signal strength in a 10-second sliding window. This RMS operation is illustrated in Figure 9 on the raw (original) and filtered (IIR Butterworth) strain gage data from the previous examples.

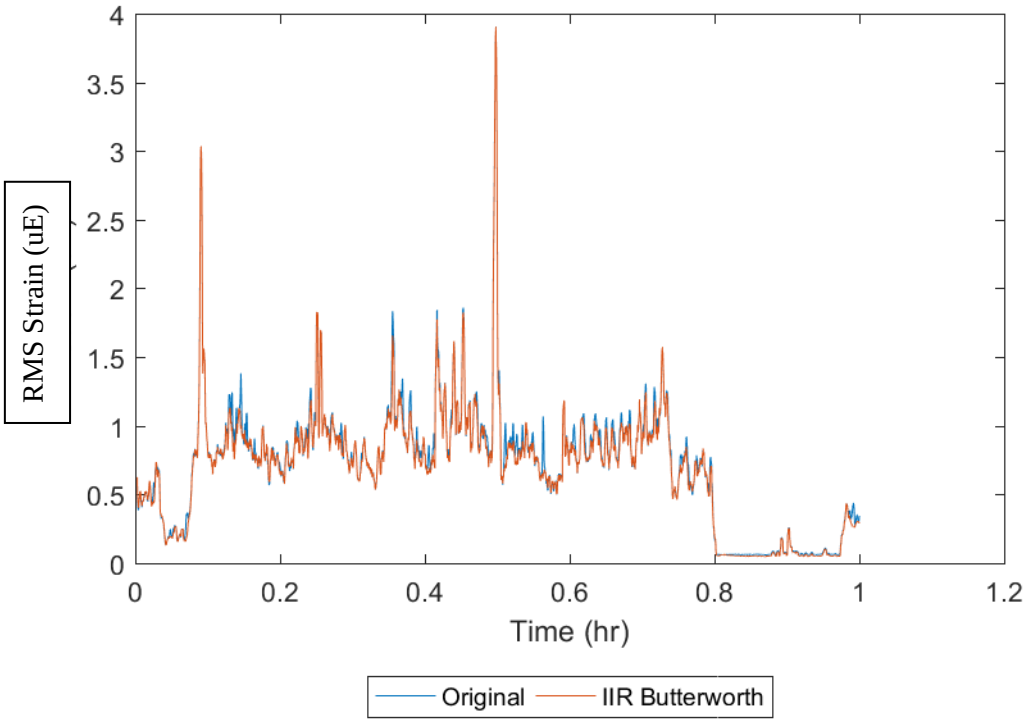

Figure 9. Sliding Window RMS

Figure 9 shows the relative signal strength during a 10-second span of time. A 10-second window is useful because it helps compress the data (10 seconds is 5120 data points). The 10-second window is shifted by 1 second each increment, such that the first RMS window is T = 0 to T = 10, then the next RMS window is T = 1 to T = 11. This process identifies when the data signal is strongest, when the signal is weak, and when there are relative changes in signal strength. The 10-second window is useful because it is a manageable length of time to analyze in finite element models of a full fuel assembly. The intent is to eventually select a number of 10-second windows of truck, ship, and railroad data as validation cases for the finite element analysis models that support this campaign.

This page is intentionally left blank.

5. FATIGUE DAMAGE

Strain gages were used to directly measure strain that occurred on the cladding at a number of select locations. In total, 37 strain gages were used on three different fuel assemblies. Each strain gage has a data channel recorded by the data acquisition system. While the peak strain to occur over time is an important value to know, the phenomenon of fatigue and the potential for a fatigue failure of the cladding from accumulated damage from low-amplitude shock and vibration is also of interest.

PNNL developed analysis tools to assess the fatigue damage at each strain gage location based on the strain gage signal. The fatigue damage calculation method used the ASTM E1049 rainflow-counting procedure to calculate the amplitude and number of fatigue cycles, and it uses Miner's Rule to calculate damage, based on a selected S-N (Stress-cycle) curve. In this application, the S-N curve is defined in terms of strain-cycle, but the two types of fatigue curves are equivalent. The final fatigue damage can be expressed as a *damage fraction*, which represents how much of the total fatigue life has been used during a certain period of time, or the damage can be expressed as a *fatigue life*, which represents how long the cladding is expected to survive under constant exposure to a given load.

Preliminary strain gage data from the ENSA/DOE test campaign were used to construct a 34-hour data set to test PNNL's fatigue damage calculation tools. The magnitude and number of strain cycles are representative of the heavy-haul truck cladding strain data, but the actual heavy-haul truck data were not available in time to be included in this report. The peak damage fraction calculated from this data set should be a good estimate of the peak heavy-haul damage fraction, and a reasonable estimate of the order of magnitude for all transportation modes. A final fatigue assessment for all transportation modes will be completed next year.

Figure 10 shows the fatigue evaluation in terms of damage fraction. The data are processed in 1-hour blocks, so the damage fraction represents the accumulated damage over 1 hour of shock and vibration loading. The highest damage fraction is on the order of 1E-9, and failure is expected when the damage fraction reaches 1.0. That can be interpreted to mean that the strongest hour of shock and vibration to occur during the 34-hour period would have to continue for 1E+9 hours before failure is expected to occur in the cladding. This is on the order of 100,000 years of continuous travel. The lowest damage fraction hours in Figure 10 could indicate that the conveyance is stopped or idling. In this method of calculating fatigue damage, the damage for any real strain gage signal would never be zero. Background noise in the data acquisition system would provide low-amplitude cycles and the S-N curve is defined to infinite cycles and infinitesimally small strain values. In assessing the damage for a real data set, the global positioning system (GPS) data will be evaluated to determine when the conveyance was stopped so the system noise threshold can be identified.

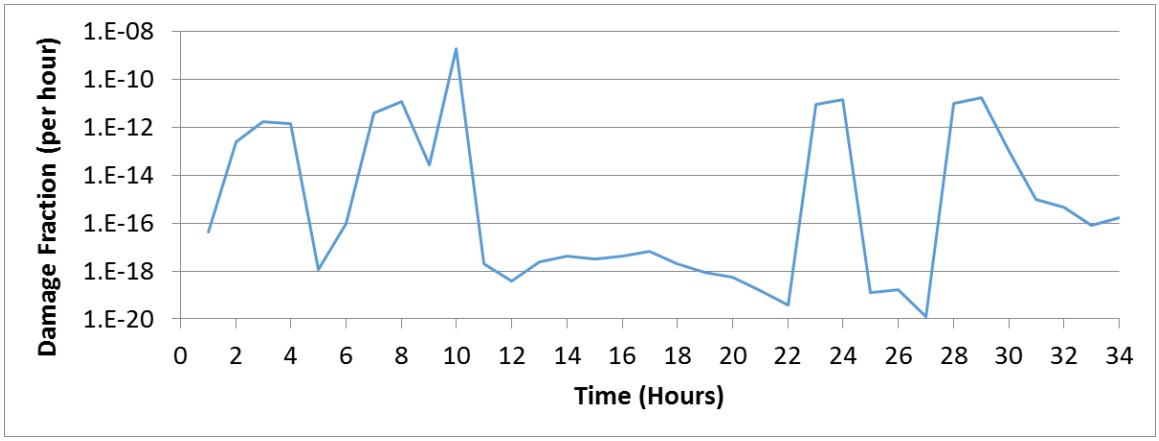

Figure 10. Illustration of Cladding Damage Fraction in a 34-Hour Data Set

The same fatigue data are presented as fatigue life in Figure 11, which inverts the shape of the curve. In this representation, the most limiting fatigue life is on the order of 1E+7 days, which is on the order of 10,000 years. The precise fatigue life calculation value for this data set falls between 10,000 years and 100,000 years, which is sufficient to estimate that cladding is not sensitive to the shock and vibration loading environment defined in the data set.

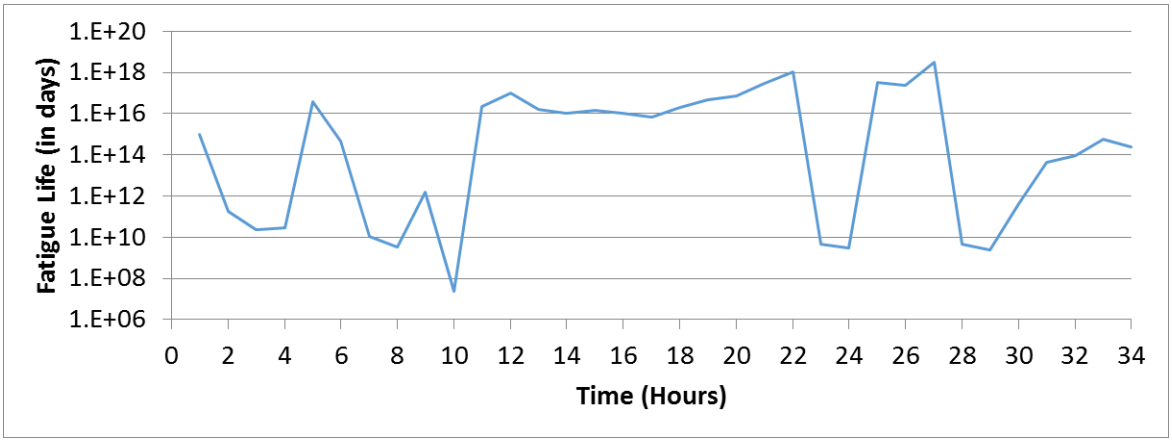

Figure 11. Illustration of Fatigue Life in a 34-Hour Data Set

The magnitude of the high fatigue life values can be checked using the S-N curve in Figure 12 and by making assumptions about the amplitude and frequency of a hypothetical constant vibration. If we assume the cladding strain experiences a hypothetical constant vibration with an amplitude of 100 µE, the corresponding number of cycles to failure is about 1E+10. If we assume that hypothetical constant vibration has a frequency of 60 Hz, 1 hour of exposure would cause 2E+5 strain cycles, and cause an accumulated damage fraction of 2E+5/1E+10, or 0.00002. This level of hypothetical constant vibration would be expected to cause fatigue failure after 50,000 hours, or just under 6 years of continuous vibration. The damage calculated from the data set is 3 to 4 orders of magnitude below that hypothetical vibration value. If we instead assume a 10 µE constant vibration with a frequency of 60 Hz, the fatigue life goes up to about 1,000,000 years. Roughly speaking, the fatigue damage predicted from the data set is comparable to the damage that would occur during a 60 Hz vibration with an amplitude between 10 and 100 µE, and this matches reasonably well with the current understanding of the test data across all modes of transportation.

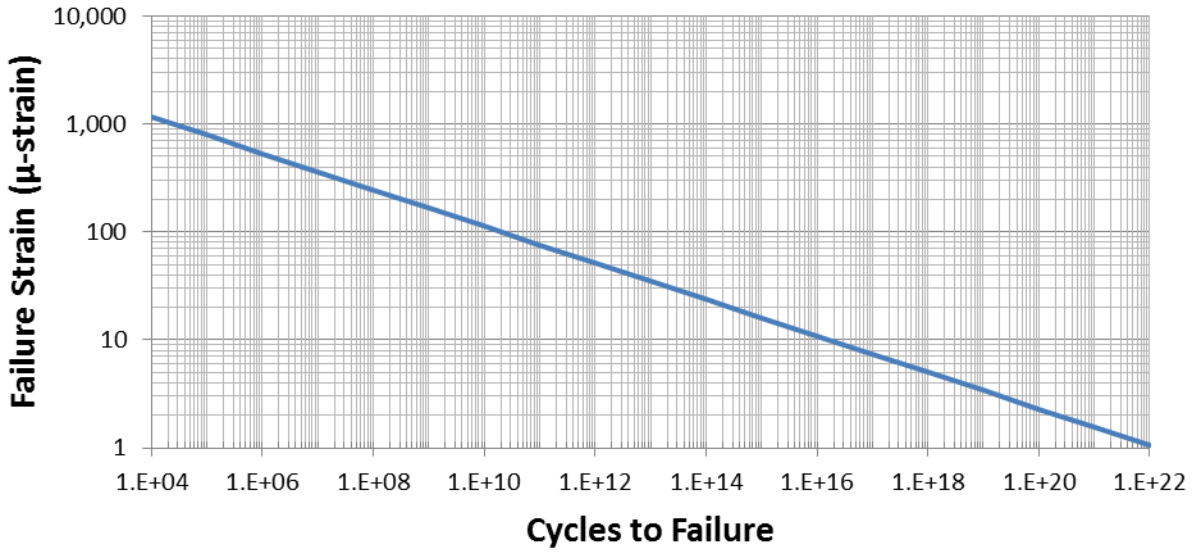

Figure 12. Fatigue Design Curve for Irradiated Zircaloy (O'Donnell 1964)

Another consideration in the cladding fatigue evaluation is the Cyclic Integrated Reversible-Bending Fatigue Tester (CIRFT) test data from Oak Ridge National Laboratory. The latest report to reference is the *FY 2017 Status Report: CIRFT Data Update and Data Analyses for Spent Nuclear Fuel Vibration Reliability Study* (M3SF-17OR010201026; Wang et al. 2017). The report provides power law regression curves on fatigue strength data for a number of different spent fuel samples. Figure 13 compares the latest power law regression curves to the O'Donnell fatigue design curve. The O'Donnell curve is more conservative in the range of 1E4 cycles to 1E9 cycles, but all of the regression curves eventually cross the O'Donnell curve at much higher cycles (one curve crosses at 1E12 cycles, the other regression curves cross beyond 1E16 cycles).

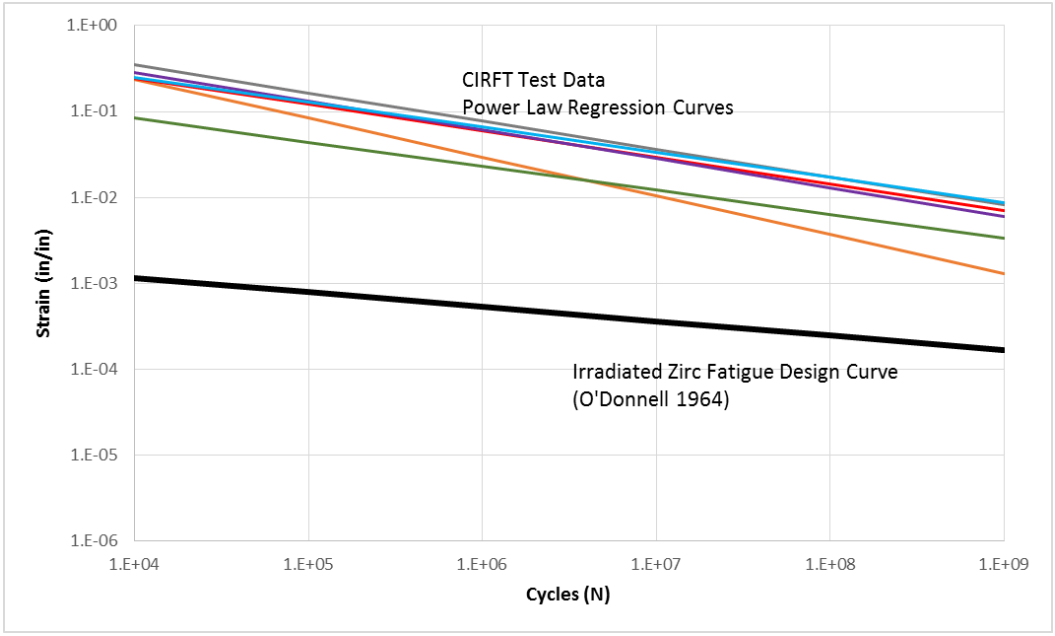

Figure 13. Comparison of Irradiated Zirc Fatigue Design Curve to CIRFT Fatigue Curves

The CIRFT regression curves are potentially misleading because the underlying data are limited in the number of cycles that were tested. Most of the CIRFT testing was halted near 1E7 cycles, which is about 50 hours of a hypothetical 60 Hz vibration. In Figure 13, the regression curves between 1E7 and 1E9 cycles represent an extrapolation from lower cycle data. From Figure 12, the 100 microstrain cycles to failure is about 1E10 cycles, so the CIRFT data are limited to orders of magnitude away from the region of interest to the strain gage data set. The CIRFT test is not capable of testing 1E10 cycles, because it would take far too much time to complete. In fact, testing 1E10 cycles seems to be outside the practical range for any type of mechanical test. A rotating shaft turning at 3600 rpm could achieve a 60 Hz repeating load cycle, but it would take 6 years to achieve 1E10 cycles. The O'Donnell design curve does not represent raw data; it was constructed from experimental data using conservative assumptions. More investigation into the O'Donnell design curve is needed to determine how credible it is in the high-cycle range. Because the O'Donnell design curve was constructed using conservative assumptions, it is the current best option for calculating damage in the low-amplitude, high-cycle range that is expected in all transportation modes.

The uncertainty in the S-N curve means the final conclusion regarding fatigue damage needs to be more carefully crafted than simply reporting the calculated fatigue life. Publicly stating that the cladding is expected to survive 100,000 years of continuous normal transportation shock and vibration loading might be effective for some audiences, but problematic for others. The fatigue damage is actually so low that making a credible determination of fatigue life is impossible. The current conclusion from this data set is that the fatigue damage is approximately zero. The final assessment next year will include a discussion of the limitations of our knowledge in high-cycle, low-amplitude fatigue to provide necessary context.

6. EFFECT OF RUBBER PADDING

The ENSA cradle structure was designed for generic, multi-modal transportation. The cask and cradle were lifted by crane from one conveyance system to another. In each case, a rubber pad was placed between the bottom of the cradle and the conveyance deck to ensure a high effective friction coefficient between the cradle and its conveyance. The use of a rubber mat in this situation is standard practice in the shipping industry but it was not specified by ENSA as a transportation requirement. Other examples of railcar spent nuclear fuel package cradle structures are directly welded to the railcar deck, so the presence of a rubber mat may be design-specific.

The rubber mat was suspected to influence the load transmission through the conveyance system. During testing at TTCI, additional accelerometers were added at one corner of the cradle; one accelerometer was glued to the railcar deck and another accelerometer was glued to the cradle structure. The two accelerometers were as close as practically achievable to each other, and a comparison of their signals is expected to be a reasonable estimate of the effect of the rubber pad on load transmission.

Acceleration data were available for "Single Bump," "Crossing Diamond," and "Hunting" tests, wherein *z*-axis acceleration of the railcar and cask frame were each measured. Frequency domain content of the acceleration data for each test was extracted using a Fast Fourier Transform algorithm. Time-domain input data to the Fast Fourier Transform algorithm was left unfiltered to preserve high-frequency content, although it was determined that a significant majority of signal content exists below 100 Hz.

Figure 14 shows the ratio of the discrete Fourier Transform of the cradle acceleration signal (a_{frame}) to the car acceleration signal (a_{car}). The discrete Fourier Transform of each signal was smoothed by a 100-point moving average prior to calculating the ratio to reduce spurious data. The mean, maximum, and minimum data were calculated from all 45 trials of the three tests (Single Bump, Crossing Diamond, and Hunting) for which acceleration data was available. Data beyond 100 Hz up to Nyquist frequency (600 Hz, or 300 Hz for Hunting tests) were truncated because the ratio remains close to 1 after this point. Clearly visible in Figure 14 are regions of amplification from 0–20 Hz, and attenuation from 20–60 Hz. Beyond 60 Hz, the ratio remains close to unity. Within the region of amplification, two peaks are visible approaching 0 Hz (r = 1.87), and at 13.2 Hz (r = 1.89). Within the region of attenuation, two troughs are visible at 30.4 Hz (r = 0.31) and 49 Hz (r = 0.30).

Figure 14 indicates that the pads affect transmission of motion from the railcar deck to the base of the cradle. Evidence of this frequency-dependent load transmission behavior should also be apparent in the main set of test data. Accelerometers were located at various locations on the railcar deck, cradle, cask, and within the cask, so amplification and attenuation between the different levels of the structure and at different frequency ranges should be captured in the data.

The extra TTCI accelerometers appear to have provided very valuable insight into the load transmission behavior of the rubber pad. We will look for confirmation of this phenomenon in the test data next year, and plan to include this phenomenon in upcoming numerical models of the conveyance system.

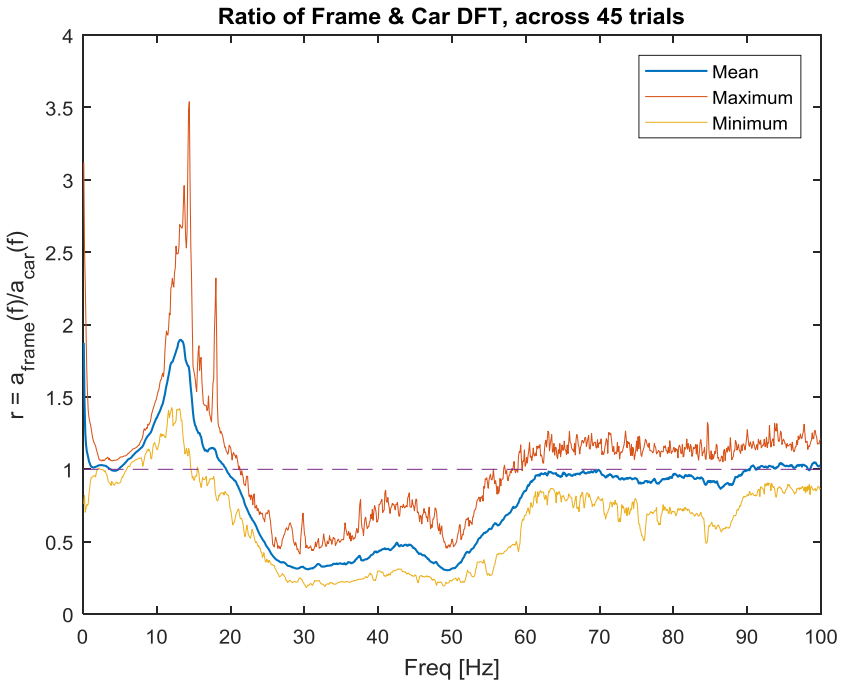

Figure 14. Acceleration Ratio

7. CONCLUSIONS

A pre-test prediction of the pitch and bounce test was made using numerical models. This test was conducted at TTCI in August 2017, but the data were not yet available at the time of this writing. The models predicted a peak cladding strain of about 300 μE. This will be compared in detail with the test data next year to determine the accuracy of the existing models and determine whether model refinement is needed to achieve better agreement with the test results.

Modeling and analysis of the simulated fuel assemblies used in testing suggest that the dynamic response of the simulated assemblies will have two characteristic frequencies. A 5 Hz response frequency is attributed to the nylon pads and rigid body motion of the simulated fuel assembly mass. A 55 Hz response frequency is attributed to the first bending mode shape. These frequencies may appear in the basket accelerometer signals or elsewhere in the data set.

Data processing is a major challenge in this project, and PNNL has developed an initial set of data processing tools to analyze the many terabytes of data as they become available. Band-pass filtering is used to eliminate noise and drift. The RMS operation on a sliding window is used to measure relative signal strength in a 10-second period. Ten seconds is a reasonable amount of time for detailed modeling of the fuel assembly, so a goal is to identify a selection of interesting 10-second periods of data across all channels.

Calculating fatigue damage using strain gage signals was explored, and all the necessary software tools were developed. A strain gage data set similar to the ENSA/DOE test campaign data was processed to calculate fatigue damage fraction and fatigue life. From this data set, we predicted that the fatigue damage for normal conditions of transport will be approximately zero when the test campaign data are evaluated next year.

The effect of the rubber pads placed between the ENSA cradle and the railcar deck was evaluated using extra accelerometer data collected at TTCI. The pads appear to have a frequency-dependent effect on the transmission of loads from the railcar deck to the cradle. At low frequencies, below 20 Hz, there is an amplification of loads up to a factor of about 2. In a higher band of frequency, 20 Hz to 60 Hz, there is attenuation down to a factor of about 0.3. This is significant enough that it should be apparent in the main set of data. If it is confirmed, this phenomenon is significant enough that it needs to be included in future dynamics models of the conveyance system.

This page is intentionally left blank.

8. REFERENCES

Jensen, P. J., N. A. Klymyshyn, and S. B. Ross. 2017. "Spent Nuclear Fuel Transportation: Rail Conveyance Transmissibility." ANS International High-Level Radioactive Waste Management, American Nuclear Society, La Grange Park, IL.

Klymyshyn, N. A., P. J. Jensen P J, and D. Garrido 2017. "Rail Package Transportation Loads Transmitted to Spent Nuclear Fuel Assemblies." ANS International High-Level Radioactive Waste Management, American Nuclear Society, La Grange Park, IL.

McConnell, P. E., R. Wauneka, S. Saltzstein, and K. Sorenson. 2014. *Normal Conditions of Transport Truck Test of a Surrogate Fuel Assembly*. Sandia National Laboratory, Albuquerque, New Mexico.

O'Donnell, W. J. and B. F. Langer. 1964. "Fatigue design basis for zircaloy components." Nuclear Science and Engineering (20):1–12.

Wang J.-A., H. Wang, B. B. Bevard, J. M. Scaglione. 2017. *FY 2017 Status Report: CIRFT Data Update and Data Analyses for Spent Nuclear Fuel Vibration Reliability Study*. ORNL/SR-2017/291, M3SF-17OR010201026, Oak Ridge National Laboratory, Oak Ridge, Tennessee.